Title

Adsorption of Dimethyl Methylphosphonate on MoO3: The Role of Oxygen Vacancies

Journal

The Journal of Physical Chemistry C, 120(51)

ISSN

1932-7447

Authors

Head, Ashley R

Tsyshevsky, Roman

Trotochaud, Lena

et al.

Publication Date

2016-12-29

DOI

10.1021/acs.jpcc.6b07340

Peer reviewed

Adsorption of Dimethyl Methylphosphonate on MoO_3: The Role of Oxygen Vacancies

Ashley R. Head,[1] Roman Tsyshevsky,[2] Lena Trotochaud,[1] Yi Yu,[1,3] Line Kyhl,[1,4] Osman Karslıoğlu,[1] Maija M. Kuklja,[2,] Hendrik Bluhm[1,*]*

[1] Chemical Sciences Division, Lawrence Berkeley National Laboratory, Berkeley, CA 94720

[2] Materials Science and Engineering Department and [3] Department of Chemistry and Biochemistry, University of Maryland, College Park, MD 20742

[4] iNANO, University of Aarhus, DK-8000 Aarhus C, Denmark

KEYWORDS: ambient pressure X-ray photoelectron spectroscopy, density functional theory, chemical warfare agent simulant, metal oxide hydroxylation

Abstract

Dimethyl methylphosphonate (DMMP) is a common chemical warfare agent simulant and is widely used in adsorption studies. To further increase the understanding of DMMP interactions with metal oxides, ambient pressure X-ray photoelectron spectroscopy was used to study the adsorption of DMMP on MoO_3, including the effects of oxygen vacancies, surface hydroxyl groups, and adsorbed molecular water. Density functional theory calculations were used to aid in the interpretation of the APXPS results. An inherent lack of Lewis acid metal sites results in weak interactions of DMMP with MoO_3. Adsorption is enhanced by the presence of oxygen vacancies, hydroxyl groups, and molecular water on the MoO_3 surface, as measured by photoelectron spectroscopy. Computational results agree with these findings and suggest the

formation of methanol through several possible pathways, but all require a proton transferred from a hydroxyl group on the surface.

Introduction

Organophosphonates represent an important class of molecules due to their effectiveness as pesticides and nerve agents.[1] Currently, there is great interest in understanding the interaction between these molecules and surfaces so new materials can be developed for personal protective devices, molecular sensors, and catalysts for the destruction of these compounds.[1] Dimethyl methylphosphonate (DMMP) is frequently used as a model compound in adsorption studies of chemical nerve agents.[1] While much less toxic than the nerve agent sarin, DMMP retains the phosphoryl group (P=O), methyl group, and an oxy group (Figure 1a,b). In the search for new materials for applications and a better understanding of DMMP surface chemistry, especially on metal oxides, adsorption studies with a focus on analyzing surface species have been conducted on TiO_2,[2-8] ZnO,[2] Al_2O_3,[2,9-11] MgO[2,9] WO_3,[2,5] La_2O_3,[9] Fe_2O_3,[9,12,13] CeO_2,[14] SiO_2,[12,15] Y_2O_3,[16] and combinations of these as supported metal oxides.[17,18] Several techniques have been used to investigate the surface species, including infrared (IR) spectroscopy,[2,4-10,12-18] Raman spectroscopy,[18] X-ray photoelectron spectroscopy (XPS),[3,6,14,16,17] inelastic tunneling spectroscopy,[11] temperature programmed desorption (TPD),[3,12,14] Auger electron spectroscopy,[12] X-ray diffraction,[17] and ion chromatography.[17] The results of these studies show that DMMP binds to metal oxides at room temperature primarily through the phosphoryl oxygen to Lewis acid metal sites on the surface, namely under-coordinated metal atoms inherent to the structure or as surface defects. Hydroxyl groups on the surface are the second favored binding site.

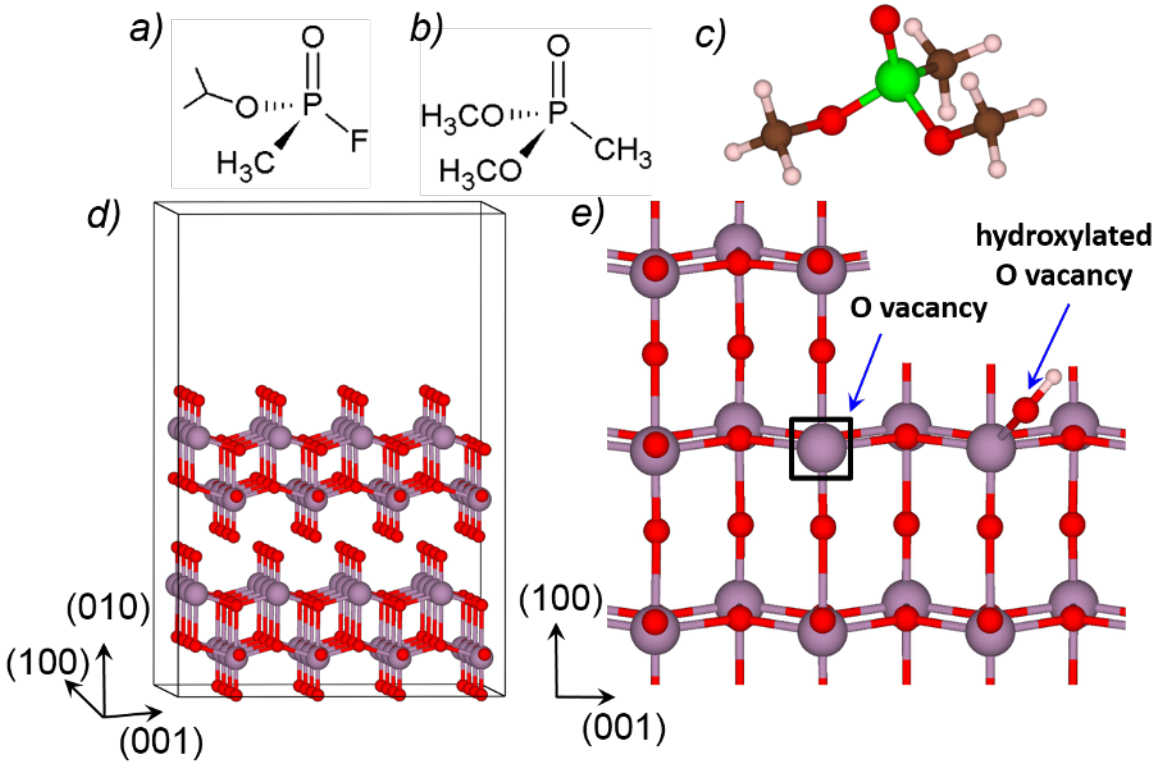

Figure 1. (a) Chemical nerve agent sarin and (b) dimethyl methylphosphonate (DMMP), (c) structure of gas phase DMMP, (d) slab model of the MoO_3(010) surface, and (e) surface structure of MoO_3, including an oxygen vacancy and a hydroxylated oxygen vacancy. P atom is green, C atoms are brown, H atoms are beige, O atoms are red, and Mo atoms are lilac.

In light of the adsorption and reactivity of DMMP with other metal oxide surfaces, we have chosen to explore the interaction of DMMP on a polycrystalline MoO_3 oxide surface, which contrasts with other metal oxides that have been studied since the MoO_3 surface structure inherently lacks under-coordinated metal atoms. As shown in Figure 1d, the bulk structure of MoO_3 consists of bilayers with hexagonally coordinated Mo atoms that are O-terminated and is often considered rather chemically inert.[19] Computational studies on the adsorption of small molecules, such as oxygen,[20] water,[21] nitric oxide,[22] and small hydrocarbons,[23] show that the interaction of adsorbates with a stoichiometric MoO_3 surface are typically weak Van der Waals interactions. However, the presence of oxygen vacancies on the surface results in under-coordinated Mo^{5+} atoms (cf. Figure 1e) and increases the adsorption and reactivity of molecules at

these sites.[22] MoO_3 serves as a catalyst in several industrial reactions, such as the dehydrogenation of alcohols[24-26] and the oxidation of propene,[27] with studies suggesting that oxygen vacancies play a role in the catalytic activity.[19,24] While oxygen vacancies can exist as point defects in MoO_3, under certain conditions, they tend to aggregate to form mixed valence phases or structurally ordered, oxygen-deficient phases known as Magnéli phases.[28]

Here, we have used ambient pressure X-ray photoelectron spectroscopy (APXPS) to compare the room temperature DMMP adsorption on a polycrystalline MoO_3 surface and a MoO_3 surface containing oxygen vacancies and OH groups. This technique allows for the collection of *in situ* X-ray photoemission (PE) spectra of a substrate under pressures in the Torr range and provides insight on pressure-dependent adsorption behavior.[29-31] We found that DMMP does not interact strongly with the O-terminated surface of MoO_3. Introducing oxygen vacancies results in Magnéli phases, hydroxyl groups, and molecularly adsorbed water. These surface features were found to enhance DMMP adsorption. Although the majority of the DMMP molecules physisorb intact, the C 1s spectra indicate some carbon loss. Density functional theory (DFT) calculations to simulate the adsorption process, decomposition reactions, and core level spectra suggest that methanol is formed by reaction with surface hydroxyl groups and desorbs from the surface, in agreement with the APXPS measurements.

Experimental Details

Materials and Methods

The experiments were conducted at the APXPS end station[32] of the 11.0.2 beamline[33] at the Advanced Light Source at Lawrence Berkeley National Laboratory. The end station is equipped with a chamber for sample preparation and an analysis chamber. The base pressure of both chambers was better than 5×10^{-9} Torr. A conical aperture with a diameter of 0.2 mm is the entrance from the analysis chamber to the differentially-pumped electrostatic lens system[34] of the electron energy analyzer, allowing *in situ* XPS measurements up to pressures of several Torr.

In the preparation chamber, a piece of Mo foil (99.99% Alpha Aesar), was cleaned with one Ar^+ ion sputter cycle (5 mA emission current, 1.5 keV, 1 x 10^{-5} Torr Ar, 5 min) followed by annealing for 5 min at 900 ºC. The MoO_3 surface was prepared by heating the foil to 430 ºC for 10 min in 35 Torr of O_2 followed by cooling to 100 ºC under the same oxygen environment. To promote the hydroxylation of surface defect sites, the surface was exposed to 10 Langmuir (L) of water. Using the known inelastic mean free path of the photoelectron in MoO_3 at 200 eV kinetic energy and the ratio between the hydroxyl and oxide peak intensities, the hydroxyl coverage was estimated to be about 10% of a monolayer. To prepare MoO_3 with more oxygen vacancies, a second sample was prepared, briefly sputtered (1 x 10^{-5} Torr Ar, 1 keV, 5 mA, 3 min, <~6.2 x 10^{12} Ar^+ cm^{-2} s^{-1}), and exposed to 10 L of water. The hydroxyl coverage was estimated to be about 30% of a monolayer for this sample. By collecting PE spectra at different areas of the sample, the surface was found to be homogenously MoO_3 with a consistent amount of Mo^{5+}. DMMP (>97%, Fluka) was degassed via freeze-pump-thaw cycles and was introduced into the analysis chamber via a leak valve.

Electrons were collected at an angle 42º from the sample normal. To minimize photon-induced changes to the substrate and adsorbed DMMP, each spectrum was taken at a new location on the sample, so all spectra presented are free from photon-induced effects. The Supporting Information further discusses these photon-induced changes. The photon energies were chosen to yield a photoelectron kinetic energy of 200 eV for all elements, thus probing the same depth. The energies used were 340 eV for P 2p, 435 eV for Mo 3d, 490 eV for C 1s, and 735 eV for O 1s. Each spectrum on the MoO_3 substrate was calibrated by the Mo $3d_{5/2}$ peak at 232.5 eV.[35] Due to a large shift of the Mo $3d_{5/2}$ in the sputtered MoO_3 sample (OH-MoO_3), the C 1s and P 2p spectra of this system were shifted to align with those of the pristine MoO_3 sample; more details are provided in the Supporting Information. A Shirley background was removed from the Mo 3d spectra, and a polynomial background from all others. The peaks were fit using Voigt functions. The spin-orbit components of the P 2p spectra were constrained to have the same peak widths, a 2:1 area ratio, and a binding energy separation of 0.85 eV.[36] The components

of the C 1s spectra were constrained to have identical peak widths. The combined beamline and electron energy analyzer resolution was better than 350 meV.

DFT Calculations

Among the various crystal structures and surface terminations of MoO_3, the (010) termination of the α-phase has been found to be the most thermodynamically stable[35] in both experimental[37,38] and theoretical[20,23,39-41] studies. Hence, this surface was used in our computational simulations. This common polymorph of molybdenum trioxide has an orthorhombic unit cell with the lattice constants of a= 3.96 Å, b= 13.86 Å, c= 3.70 Å.[42,43] The atomistic structure consists of bilayers parallel to the (010) plane that are bound by mainly electrostatic and weak van der Waals (vdW) interactions. Recent theoretical studies emphasized the importance of vdW contributions in density functional theory (DFT)[44,45] calculations to reproduce an accurate crystal structure of α-MoO_3.[46,47] On the other hand, formation energies of surface oxygen vacancies on α-MoO_3 (010) surface were found to depend on the accurate treatment of the electron localization.[20]

In the current study, solid state periodic calculations were performed by employing DFT with the optPBE-vdW[48-50,51,52] functional, which includes corrections for van der Waals interactions, as implemented in the VASP code.[53-55] The projector augmented wave (PAW) pseudo-potentials[56] were used. In calculations of a stoichiometric MoO_3 crystal, the convergence criterion for the total energy was set to 10^{-5} eV, and the maximum force acting on each atom in the periodic supercell was set not to exceed 0.02 eV/Å. The 2×6×6 Monkhorst–Pack k-point mesh with a kinetic energy cut-off of 520 eV was used. The optimized lattice constants of the orthorombic unit cell with the Pbnm space group (Figure S7) were a= 3.99 Å, b= 14.3 Å, c= 3.73 Å, agreeing with experimentally determined[57,58] within 3%.

In the MoO_3 surface calculations (cf. Figure 1d), the model surface slab was cut out of the bulk MoO_3 structure to form the (010) surface, with the supercell lattice vectors of a =14.92 Å, b =15.97 Å, and c =33.50 Å. A vacuum layer of 20 Å placed on top of the MoO_3 (010) surface

served to minimize interactions between the supercells in the z-direction and to avoid any significant overlap between wave functions of periodically translated cells. An oxygen vacancy on the MoO_3 (010) surface was simulated by removing one of the terminal oxygen atoms from the top layer of 256 atom supercell (cf. Figure 1e), which requires less energy than removing bridging oxygen atoms.[20,59]

To model adsorption and decomposition of DMMP on a hydroxylated MoO_3 (010) surface, four terminal oxygen atoms were replaced by hydroxyl groups (Figure 1e), as it has been shown previously that hydrogen adsorbs more strongly to the terminal rather than bridging oxygen[Error! Bookmark not defined.,Error! Bookmark not defined.] due to the strong covalent interaction of H 1s and O 2p atomic orbitals.[Error! Bookmark not defined.] Surface supercell calculations were performed at the Gamma point only, with the convergence criteria for electronic and ionic steps set to 10^{-5} eV and 0.03 Å/eV, respectively.

Calculations with the PBE+*U* method[60,61] were performed to reveal the effect of the electron localization on the adsorption of DMMP on the MoO_3 (010) surface. A value of 6.3 for *U* parameter was taken from the study by Coquet and coworkers.[20] Our calculations revealed that PBE+*U* tends to significantly overestimate "*b*" lattice constant of the MoO_3 unit cell by ~9% due to its failure to describe correctly the vdW interactions between MoO_3 bilayers. Therefore, to probe the adsorption of DMMP on the MoO_3 (010) surface with the PBE+*U* approach, we employed the supercell that was previously built for optPBE-vdW calculations in which atoms only from the four top atomic layers were allowed to relax. The positions of the rest atoms were fixed (see the Supporting Information for more details). PBE+*U* calculations were performed at the Gamma point only with the kinetic energy cut-off set to 450 eV.

Our simulations show that geometries of pristine MoO_3 and defect-containing MoO_3 (010) surfaces as well as energies of DMMP adsorption calculated using optPBE-vdW and PDE+U functionals were found to be in satisfactory agreement. At the same time, adsorption energies obtained from DFT+*U* strongly suffer from the lack of corrections for vdW interactions. As the result, DFT+U does not perform for our task with the required accuracy, as detailed in

Supporting Information. Therefore, optPBE-vdW was chosen as the main tool for modeling decomposition reactions of DMMP on MoO_3 surfaces.

In test calculations to model the gas phase decomposition using the VASP code, a single DMMP molecule was placed in the center of a large periodic box with the cell parameters $a=b=c=20$ Å. Additionally, calculations with the B3LYP[62,63] functional were performed with the 6-31+G(d,p) basis set, as implemented in the Gaussian09 code.[64] Consistency between periodic (VASP) and molecular (GAUSSIAN) calculations lends an additional support for accuracy of the results and serves as validation of obtained conclusions.

Minimal energy paths in the VASP periodic calculations were obtained with the nudged elastic band method[65] with five intermediate images. Atomic positions were relaxed using conjugate gradient and quasi-Newtonian methods within a force tolerance of 0.05 Å/eV. A Hessian-based Predictor-Corrector integrator algorithm[66,67] was employed to conduct intrinsic reaction coordinate computations in the Gaussian09 code. The stationary points corresponding to the energy minimum were positively identified by having no imaginary frequencies and the transition states had exactly one imaginary frequency. Calculations of vibrational frequencies in VASP, especially for such a large system, is a tedious procedure. Therefore, we calculated vibrational frequencies of transition state structures for several possible reaction pathways of methanol elimination (see Table S1 of Supplementary Information). In calculations of vibrational frequencies, only ionic positions of DMMP atoms and surface hydroxyl groups were allowed to be changed, whereas positions of other atoms were fixed.

Results

Ambient pressure XPS

Before dosing DMMP, the oxidized Mo foil was characterized by measuring the Mo 3d and O 1s spectra (cf. Figures 2a and 3a), which agree with those of MoO_3 found in the literature.[35] No peak corresponding to the metal substrate was detected. The binding energy of the small shoulder in the Mo 3d spectra matches that of a Mo^{5+} oxidation state.[35,68,69,70,71] While the Mo^{5+} component was found to be linked to photon-induced damage of the substrate,[72] the peak was

present also in spectra where exposure to the beam was minimized (see Supporting Information). Oxygen vacancies on the surface give rise to Mo^{5+} species, either in the form of point defects or extended oxygen-deficient phases,[28] and these Mo^{5+} species are feasibly due to defects, such as grain boundaries, in the polycrystalline foil from which MoO_3 was grown. Additionally, in a previous report of single crystal MoO_3, it was difficult to completely oxidize the surface to MoO_3 and remove all oxygen vacancies.[35] Therefore, we assume that the prepared surface contained some oxygen vacancies prior to photon beam exposure.

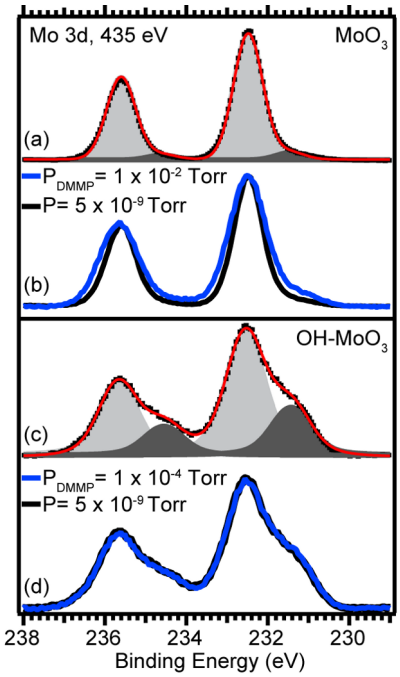

Figure 2. Mo 3d PE spectra of (a) pristine MoO_3, (b) pristine MoO_3 (black) and under a DMMP pressure of 1 x 10^{-2} Torr (blue), (c) OH-MoO_3 as prepared, and (d) OH-MoO_3 as prepared (black) and under a DMMP pressure of 1 x 10^{-4} Torr (blue). Voigt functions of the spectral fits (red lines) are shaded with the dark grey representing Mo^{5+} and the lighter grey representing Mo^{6+}. All spectra are normalized to their maximum intensity.

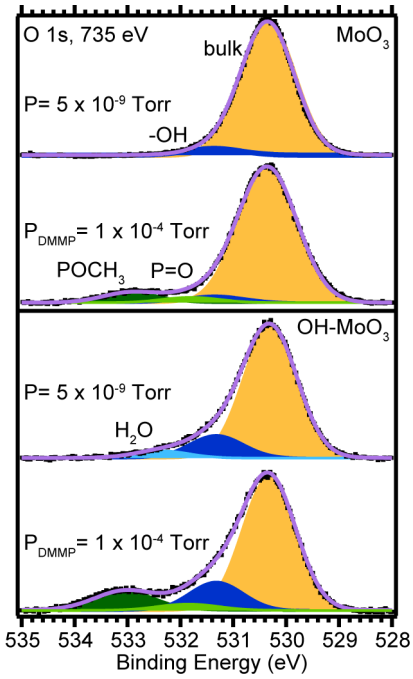

Figure 3. O 1s PE spectra of (a) pristine MoO_3 , (b) pristine MoO_3 under a DMMP pressure of 1 x 10^{-4} Torr, (c) OH-MoO_3 as prepared, and (d) OH-MoO_3 under a DMMP pressure of 1 x 10^{-4} Torr. The spectra are normalized to their maximum intensity. The black dots are the data points, the lilac line is the fit of the Voigt functions (yellow is bulk MoO_3, blue is hydroxyl groups, light blue is molecular water, dark green is phosphoryl oxygen, and light green is methoxy oxygen).

Oxygen vacancies often promote water dissociation to form a hydroxyl at the vacancy site and transferring the second proton to a neighboring surface oxygen atom. For many oxide surfaces, this process is facile even at water vapor pressure below 10^{-8} Torr.[31] The O 1s spectrum of the pristine MoO_3 foil in Figure 3a shows the metal oxide component and a small binding energy shoulder about 1 eV higher than the bulk oxide, consistent with the presence of surface hydroxyl groups.[31,73,74] This hydroxyl peak has been assigned previously on MoO_3 samples prepared under UHV conditions.[35,68,70,71,75] The other possibility is that this peak corresponds to the oxygen deficient Magnéli phases. While there is little literature on the O 1s binding energy of Magnéli phases of MoO_3, two factors discount this assignment. (i) The O 1s binding energy of the Mo^{6+} and Mo^{4+} oxides are within a few tenths of an eV of each other,[35,71] and it is likely that the intermediate oxide

state would be similar. (ii) A study of the growth of MoO_3 clusters on an Au substrate initially shows a significant amount of Mo^{5+} in the Mo 3d spectrum but no corresponding peak in the O 1s spectrum, indicating there is no significant chemical shift between Mo^{6+} and Mo^{5+} oxides. Therefore, we assign this high binding energy shoulder to hydroxyl groups, formed from a background pressure of water.

Since hydroxyl groups are inherent to our sample preparation method, we wanted to test the interaction of DMMP on a MoO_3 surface with a greater coverage of hydroxyl groups. On polycrystalline MoO_3, water adsorption and hydroxyl group formation is known to be quite low and is higher for sub-stoichiometric films.[76] Therefore, another sample with an increased number of oxygen vacancies was deliberately prepared by light sputtering in order to promote a higher hydroxylation coverage. The amount of the Mo^{5+} component has increased, as shown in the Mo 3d spectrum in Figure 2c. Sputtering has been shown to create oxygen vacancies on MoO_3, which migrate to form extended defect structures.[28,77] To encourage oxygen vacancy hydroxylation, both the untreated and sputtered surfaces were exposed to 10 L of H_2O. Correspondingly, the O 1s spectrum of this surface in Figure 3c shows an increase in the OH coverage. A third component in the O 1s spectrum of the hydroxylated MoO_3 in Figure 3c is consistent with molecular water absorbed on the surface,[31,78,79] with the peak being positioned 2.1 eV higher than the bulk peak. Though water on a room temperature metal oxide surface under UHV is uncommon,[80] it is known to occur on RuO_2[81] and MgO,[79] for example. The molecular water further suggests a larger concentration of surface hydroxyl groups since hydroxyl groups are known to induce water adsorption to surfaces.[82] Thus, this sputtered surface contains extended, oxygen deficient phases, hydroxyl groups, and molecularly adsorbed water. To distinguish between the two surfaces, the MoO_3 as prepared is referred to as pristine MoO_3, and the sputtered surface that contains more hydroxyl groups is labelled OH-MoO_3.

The substrates were gradually exposed to increasing DMMP pressures at room temperature while collecting PE spectra. The two peaks in the C 1s PE spectra (cf. Figure 4a,b) show that DMMP is adsorbing on both surfaces, with the peak at 284.5 eV assigned to the methyl group,

and the higher binding energy peak at 286.3 eV assigned to the methoxy groups.[36] Figure 4c,d shows the P 2p spectra of DMMP absorbed onto both surfaces, with the $2p_{3/2}$ and the $2p_{1/2}$ spin-orbit components resolved. The lack of additional peaks in the C 1s and P 2p spectra suggest that DMMP could be adsorbing intact. The methoxy to methyl C 1s peak area ratio is close to the expected value of 2 for the intact molecule adsorbed on pristine MoO_3, as shown in Figure 5a. However, this ratio is much lower for DMMP adsorption on OH-MoO_3, especially at lower pressures. This deviation indicates that either a volatile product containing carbon is being formed, preferentially from the methoxy groups, or that methoxy carbons are being converted to methyl carbons.

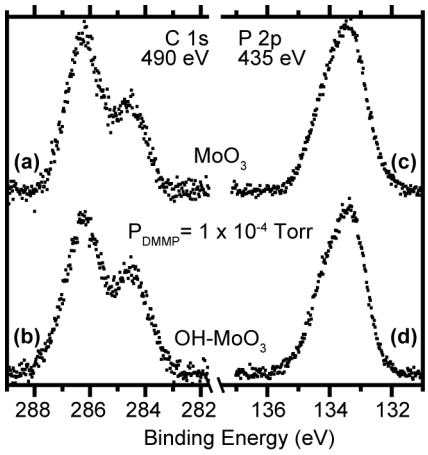

Figure 4. C 1s PE spectra of DMMP on (a) pristine MoO_3 and (b) OH-MoO_3 and P 2p PE spectra of DMMP adsorbed on (c) pristine MoO_3 and (d) OH-MoO_3 under a DMMP pressure of 1 x 10^{-4} Torr. The spectra have been normalized to their maximum intensity. Spectra of the clean surfaces are given in the Supporting Information (Figures S5a and S5b).

Peaks corresponding to the methoxy groups and phosphoryl oxygen atoms are evident in O 1s spectra of pristine MoO_3 under a DMMP pressure of 1 x 10^{-4} Torr in Figure 3b. In Figure 3d, the overlap of the hydroxyl peak with the phosporyl peak complicates the analysis of the OH-MoO_3 spectrum. The spectral fit in Figure 3d was obtained by restricting the bulk oxide (yellow curve) and hydroxyl (blue curve) peaks to the same parameters (FWHM, BE) as in the pristine MoO_3

spectrum in Figure 3a. The ratio of the DMMP peaks (green curves) were set equal to the C 1s area ratio in Figure 5a, which assumes that even if some methoxy groups are leaving, the remaining surface fragment will have a methyl and a P=O group. As discussed in the theoretical section, this assumption is reasonable. More details of the spectral fits are given in the Supporting Information. Hydroxyl groups often react with surface species, especially molecules prone to hydrolysis such as DMMP.

The O 1s spectra can be used to calculate an approximate coverage of DMMP on the pristine MoO_3 and OH-MoO_3 surfaces, using the method described in Ref. 79**Error! Bookmark not defined.**, which assumes adsorption in a 2D geometry. While we expect that in the case of pristine MoO_3 and OH-MoO_3 the surface will be rough due to the polycrystalline nature of the starting material, the method still allows for an estimate of the coverages that can be compared between the two surfaces. Details of the calculations are reported in the Supporting Information, and the results are plotted in Figure 5b. The coverage calculated from both the methoxy and phosphoryl O peaks for the pristine MoO_3 agree with each other. Since there is some methoxy loss on the OH-MoO_3 sample, the coverages calculated with this peak are slightly lower than those calculated from the P=O O 1s peak. The results in Figure 5b show that for all pressures DMMP absorption is higher on OH-MoO_3 than on pristine MoO_3.

The Mo 3d spectrum of OH-MoO_3 does not change upon DMMP adsorption (cf. Figure 2d). However, the Mo 3d spectra of the pristine surface show broader peaks at higher DMMP pressures and a higher abundance of Mo^{5+}, as seen in Figure 2b. The increase in the Mo^{5+} peak intensity is monotonic with DMMP pressure and was found not to be photon-induced, as evidenced by faster acquisition times and reproducibility in a second data set (see Figure S2).

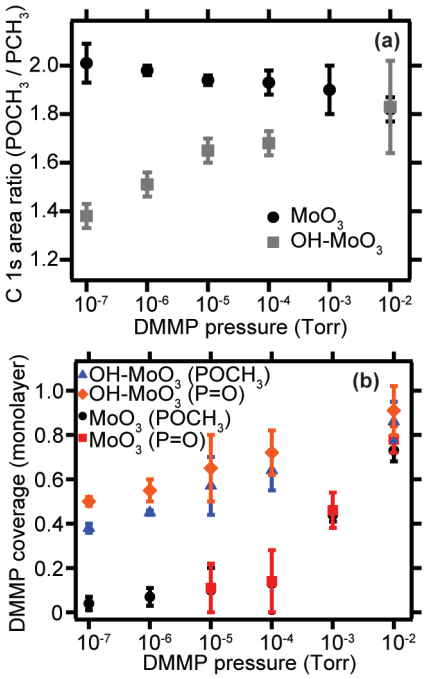

Figure 5. (a) Pressure dependence of the C 1s peak area ratio (methoxy:methyl) of DMMP adsorbed on pristine MoO_3 (black circles) and OH-MoO_3 (grey squares). (b) DMMP coverage on OH-MoO_3 calculated from the methoxy (blue triangles) and P=O (orange diamonds) O 1s peaks and on pristine MoO_3 calculated from the methoxy (black circles)P=O (red squares) O 1s peaks. The error bars originate from the peak fitting of the spectra.

DFT Calculations

The adsorption of DMMP on MoO_3 (010), the most stable surface, was modeled with DFT calculations to aid in the interpretation of the APXPS results of the polycrystalline film. Figure 6a and b shows that while DMMP will adsorb on the pristine MoO_3 (010) surface (with the adsorption energy of 20 kcal/mol), oxygen vacancies, hydroxyl groups, and a combination of these defects will enhance the chemisorption. Figure 6 also indicates that the most energetically favored interaction between DMMP and a non-hydroxylated MoO_3 (010) surface is through the phosphoryl oxygen (configuration *C1*, Figure 6a). In configuration *C1*, a new weak bond between the phosphoryl oxygen and the molybdenum atom is formed. The adsorption of the DMMP on the metal atom is accompanied by the cleavage of one of the bonds between Mo atom and surface oxygen. As a result, the oxidation state of the Mo remains 6+, which agrees with the

experiments. In the second most favorable configuration *C2* (Figure 6b), the DMMP molecule is weakly adsorbed (through physisorption) on the MoO_3 (010) surface, and no chemical bond is formed between the molecule and the oxide surface. The calculated adsorption energy for the configuration *C2* is 20.1 kcal/mol. The presence of terminal oxygen vacancies noticeably enhance DMMP adsorption, as the calculated adsorption energy of DMMP atop the under-coordinated Mo atoms in the configuration *C3* (Figure 6c) is 36.7 kcal/mol.

For DMMP on OH-MoO_3, there are two favorable configurations with adsorption energies of -35.8 kcal/mol for configuration *C4*, shown in Figure 6d, and 33.4 kcal/mol for configuration *C5*, shown in Figure 6e. In adsorption configurations *C4* and *C5*, DMMP interacts either with one or two surface OH groups through its phosphoryl oxygen. We note, that in the configuration *C4* (Figure 6d), a proton migrates from the surface to the phosphoryl oxygen of DMMP leading to a formation of H^+-DMMP cation. In addition to configurations *C4* and *C5,* we also simulated adsorption of DMMP on the hydroxylated MoO_3 (010) surface through its methoxy oxygen atoms (configuration *C6*, Figure 6f). The calculated adsorption energy for configuration *C6* is 24.6 kcal/mol.

Further, our simulations show that adsorption of DMMP on MoO_3 (010) surface containing both an oxygen vacancy and hydroxyl groups in close proximity to each other is even more energetically advantageous than the adsorption on the surface with oxygen vacancies only or hydroxyl groups only. Thus, the calculated energies of the DMMP adsorption energy on the surface with an oxygen vacancy and one hydroxyl group is 42.3 kcal/mol (configuration *C7*, Figure 6g), and on the same surface with two hydroxyl groups, the adsorption energy 47.6 kcal/mol (configuration *C7*, Figure 6g). Overall, the trend in all the adsorption energies in Figure 6 agree with larger DMMP coverage of OH-MoO_3 plotted in Figure 5b, i.e. all adsorption geometries of DMMP on oxygen deficient and/or hydroxylated surfaces MoO_3 (010) have more favorable adsorption energies than the lowest energy geometry on the pristine MoO_3.

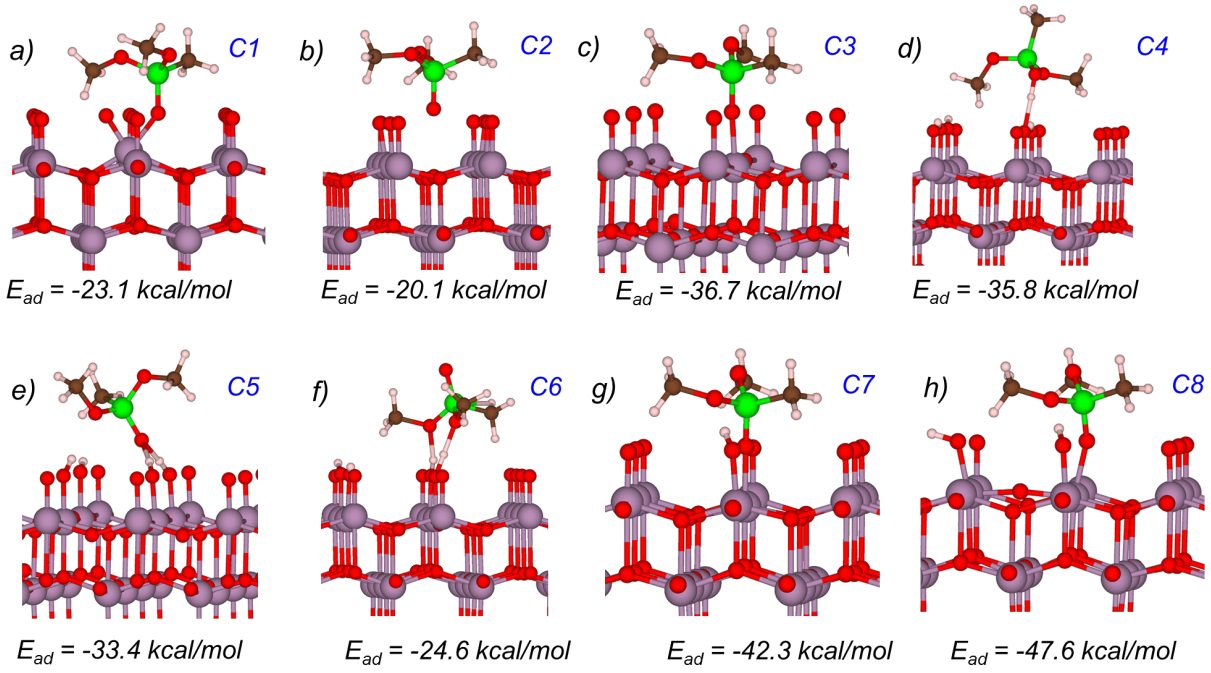

Figure 6. The structure of (a), (b) the energetically favorable configurations of DMMP adsorbed on pristine MoO_3, labelled C1 and C2, (c) preferred configurations of DMMP on the MoO_3 surface with a terminal oxygen vacancy, labelled C3, (d), (e) and (f) three preferred configurations of DMMP on OH-MoO_3, labelled C4, C5 and C6, respectively, (g) and (h) possible configurations of DMMP on MoO_3 surface with an oxygen vacancy and one and two hydroxyl groups, labelled C7 and C8, respectively. O is red, P is green, H is beige, C is brown, and Mo is lilac.

To investigate possible reasons for the loss of methoxy carbon on the OH-MoO_3 seen in Figure 5a, reasonable decomposition products and pathways were explored. We first considered DMMP decomposition in the gas phase by modeling several plausible decomposition channels, including the gas phase bond dissociation of the P-CH_3 bond (Eq. 1), the O-CH_3 bond (Eq. 2), and the P-OCH_3 bond (Eq. 3) and the elimination of methanol by intramolecular hydrogen transfer (Eq. 4).

$OP(CH_3)(OCH_3)_2 \rightarrow OP^{\bullet}(OCH_3)_2 + {}^{\bullet}CH_3$ (1)

$OP(CH_3)(OCH_3)_2 \rightarrow OP(CH_3)(OCH_3)(O^{\bullet}) + {}^{\bullet}CH_3$ (2)

$OP(CH_3)(OCH_3)_2 \rightarrow OP^{\bullet}(CH_3)(OCH_3) + {}^{\bullet}OCH_3$ (3)

$OP(CH_3)(OCH_3)_2 \rightarrow OP(CH_2)(OCH_3) + HOCH_3$ (4)

Table 1 shows that the elimination of methanol is the most energetically favorable path among these processes. Requiring 69.9 kcal/mol, this process has a 12.4 kcal/mol, 19.2 kcal/mol and 31.3 kcal/mol lower activation barrier than the O-CH_3, P-CH_3, and P-OCH_3 bond dissociation energies, respectively. These findings are consistent with a recent study, reporting methyl and methanol among other products of DMMP pyrolysis in the gas phase.[83] The same study also found that formaldehyde loss occurred via a two-step process[83] that involves complex isomerization of the molecule accompanied by an intramolecular hydrogen transfer and a rotation of functional groups (see Figure S8). Due to its intramolecular nature, the presence of surface defects hardly affects the activation barrier of the rate limiting reaction step (~65 kcal/mol) of formaldehyde elimination from DMMP proceeding through intramolecular hydrogen shift from methoxy carbon to phosphoryl oxygen. Hence we did not consider this mechanism as a potential decomposition channel on the ideal and hydroxylated MoO_3 surface despite the similar activation energy to the methanol elimination (see Figure S8).

Table 1. Calculated decomposition Energies of DMMP (kcal/mol)

Reaction	gas phase	DMMP adsorbed on						
		pristine surface		Surface with oxygen vacancy	$OH\text{-}MoO_3$ surface			Surface with oxygen vacancy and hydroxyl group
		Conf. C1	Conf. C2	Conf. C3	Conf. C4	Conf. C5	Conf. C6	Conf. C8
$P\text{-}CH_3$ (Eq 1)	89.1	97.8	90.4	-	69.7	-	-	-
$O\text{-}CH_3$ (Eq 2)	82.3	96.5	85.8	59.7	30.1[b]	29.8[b]	38.5[b]	35.6[b]
$P\text{-}OCH_3$ (Eq 3)	101.2	107.0	92.8	99.4	102.3	-	-	-
CH_3OH loss (Eq 4)	69.9[a]	78.7[a]	69.1[a]	78.[a]	76.2[c] 44.9[e]	76.1[c] 45.2[d]	74.7[c] 28.9[e] 41.6[f]	82.9[c] 40.1[d]

[a] Collected decomposition energies correspond to the highest activation barrier of the two-stage reaction of methanol formation (see Figure 7).

[b] Energies of the $O\text{-}CH_3$ bond dissociation were obtained assuming the absence of the activation barrier of the reverse reaction (Figure S9)

[c] Decomposition energies were calculated as overall reaction energies of methanol elimination (see path *II*[2] in Figure 8a).[d] The activation barrier calculated for the methanol loss reaction via surface-to-molecule hydrogen transfer shown in Figure 8a.

[e] The activation barrier calculated for the methanol loss via surface-to-molecule hydrogen transfer shown in Figure 8b, reaction pathway *IV*.

[f] The activation barrier calculated for the methanol loss via the stepwise reaction pathway *V* of Figure 8b.

The energies for the reactions in Equations 1 through 4 were calculated for DMMP on a pristine MoO_3 surface, starting from the configurations *C1* and *C2* in Figure 6a and b; the dissociation energies are provided in Table 1. Methanol loss remains the most favorable path for both configurations, with the calculated activation barrier of 78.7 and 69.1 kcal/mol (Figure 7), respectively. Dissociation of the $P\text{-}CH_3$, $O\text{-}CH_3$ and $P\text{-}OCH_3$ bonds in the lowest energy configuration *C1* requires energy that is 7-10 kcal/mol higher than that in the gas phase. Dissociation of the $P\text{-}CH_3$ and $O\text{-}CH_3$ bonds in the configuration *C2* requires about the same amount of energy as in the gas phase, whereas the energy necessary for the $P\text{-}OCH_3$ bond cleavage on the pristine MoO_3 surface is 8.4 kcal/mol lower than that in the gas phase. The relatively low adsorption energy (20-23 kcal/mol, Figure 6a and b) coupled with high activation energies required for the DMMP decomposition on the stoichiometric MoO_3 (010) surface suggest that pristine MoO_3 will likely demonstrate rather low catalytic activity towards DMMP

decomposition. This agrees well with XPS data, which shows low DMMP coverage on pristine MoO_3 and the nearly 2:1 methoxy to methyl C 1s peak area ratio (cf. Figure 5a).

Dissociation of PO-CH_3 bond in DMMP adsorbed on the oxygen deficient MoO_3 (010) surface (configuration C3, Figure 6c) requires energy, which is 22.6 kcal/mol lower than in the gas phase and 26.1 kcal/mol lower than on the pristine surface (Table 1). Furthermore, the relatively low energy of the PO-CH_3 bond cleavage (59.7 kcal/mol, Table 1) suggests that this mechanism dominates over the P-OCH_3 bond dissociation and methanol formation in the DMMP decomposition on the vacancy-rich MoO_3 surface due to the higher activation energies required for the latter two mechanisms, 99.4 kcal/mol and 78.4 kcal/mol (Table 1), respectively.

Next, the decomposition of DMMP on OH-MoO_3, the methanol loss through an intramolecular hydrogen transfer (*path II*, Figure 8a), starting from the most favorable configuration, *C4* in Figure 6d, was modeled. The calculated overall activation barrier, 76.2 kcal/mol, is similar to those obtained for the gas phase and the ideal stoichiometric surface. The surface hydroxyl groups provide new channels for the methanol elimination from DMMP via surface-to-molecule hydrogen transfer, which is illustrated as *path III* in Figure 8a. This reaction pathway requires only 44.9 kcal/mol, which is ~30 kcal/mol lower than the methanol elimination through an intramolecular hydrogen transfer. The significant drop in the activation energy for methanol loss on the OH-MoO_3 surface agrees with the XPS measurements (cf. Figure 5a). The DMMP adsorption on OH-MoO_3 also reduces the dissociation energy of the P-CH_3 and O-CH_3 bonds as compared to the gas phase and the pristine MoO_3 surface (cf. Table 1). The calculated energy of the P-CH_3 bond cleavage on the hydroxylated surface, although ~20 kcal/mol lower than that on the ideal surface, remains too high to consider this mechanism as a viable channel for the DMMP decomposition on OH-MoO_3. The O-CH_3 bond cleavage of DMMP on OH-MoO_3 is accompanied by migration of one of the surface hydrogens to the oxygen with unpaired electron (Figure S9) and has the lowest energy (30.1 kcal/mol, Table 1) among all studied pathways; this could explain the decrease in methoxy C 1s signal. However, the bond dissociation energy in Table 1 may be underestimated as it was obtained as the difference between total energies of products

and reactants assuming that reverse reaction has no activation barrier (Figure S9) A large activation barrier would preclude the removal of the methyl from the surface, in which case a change of the C 1s peak would not be expected. To refine modeling of this decomposition pathway, more comprehensive information on the decomposition products is required, but is not attainable at this point. Hence, the possibility of this pathway occurring cannot be ruled out for the time being.

We now turn our attention to the mechanisms of methanol loss starting from the less energetically favorable, but still viable, configurations *C5* and *C6* on OH-MoO_3. To study decomposition of DMMP from the configuration *C5*, we modeled three possible mechanisms (Figure S10) to seek a possible explanation for the experimentally observed change in methoxy C 1s signal. Elimination of the methanol via intramolecular hydrogen transfer requires slightly higher energy (76.1 kcal/mol, Table 1) than in the gas phase and on the pristine surface. The calculated activation barrier of the alternative mechanism via surface-to-molecule hydrogen transfer (45.2 kcal/mol, Table 2) is 30.9 kcal/mol lower. Similarly to the configuration *C4*, the presence of surface hydroxyl groups causes a reduction of the energy of O-CH_3 bond breaking by 52.5 and 56 kcal/mol as compared to gas phase and pristine surface, respectively (Table 1).

For the configuration *C6,* we also considered three possible mechanisms of the methanol formation. The first mechanism proceeds via a surface-to-molecule hydrogen transfer, shown as *path IV* in Figure 8b, and requires only 28.9 kcal/mol, which is ~17 kcal/mol lower than starting from the more energetically favorable configurations *C4* and *C5* on OH-MoO_3. The second possible channel of the methanol formation (*path V*, Figure 8b) proceeds via splitting of the O-CH_3 bond in DMMP and subsequent adsorption of the methyl group onto a surface hydroxyl (*path* V_1, Figure 8b). The calculated activation barrier of this reaction step is 41.6 kcal/mol. The methanol molecule is weakly bound to the surface, requiring only 18.3 kcal/mol for its desorption (*path* V_2, Figure 8b). The obtained energy required for methanol elimination via intramolecular hydrogen transfer (74.7 kcal/mol, Table 1) is significantly higher than the activation barriers of the former two channels. Furthermore, we examined the mechanism of the

loss of a methoxy group formed through the O-CH_3 bond cleavage and subsequent adsorption of the methyl group onto one of the terminal surface oxygen atoms (*path VI*$_1$, Figure 8b). The calculated activation barrier for this reaction step is 40.2 kcal/mol. The large energy of the following step (69.3 kcal/mol, *path VI*$_2$, Figure 8b) precludes this mechanism from contributing to the methanol loss observed in the experimental data. If this pathway does occur with the surface methoxy remaining on the surface, the experimental binding energies would be indistinguishable from those of intact DMMP adsorbed on the surface. The reaction of CH_3□ loss through O-CH_3 bond breaking in DMMP adsorbed in the configuration *C6* requires 38.5 kcal/mol (Table 1).

Finally, we studied the methanol elimination reaction from the most preferred adsorption configuration *C8* (Figure 6h), in which DMMP adsorbs on the MoO_3 (010) surface containing both oxygen vacancies and hydroxyl groups (Figure 9). The first step involves splitting the O-CH_3 bond in the DMMP molecule, transfer of the CH_3 group to a surface hydroxyl group, and surface-to-molecule hydrogen transfer (*path VII*$_1$, Figure 9). This reaction step requires 40.1 kcal/mol with the calculated reaction energy of -16.2 kca/mol. The energy of the subsequent methanol desorption from the surface (*path VII*$_2$, Figure 9) is 28.2 kcal/mol. The methanol loss via intramolecular hydrogen transfer requires 82.9 kcal/mol. The calculated energy of the O-CH_3 bond dissociation reaction is 35.6 kcal/mol.

Overall, our modeling clearly demonstrates that the surface hydroxyl groups and oxygen vacancies enhance the adsorption of DMMP on the MoO_3 surface. A significant drop in the calculated activation energies for both methanol loss and O-CH_3 bond cleavage is consistent with the reduction of the methoxy to methyl C 1s peak area ratio for the hydroxylated surface (Figure 5).

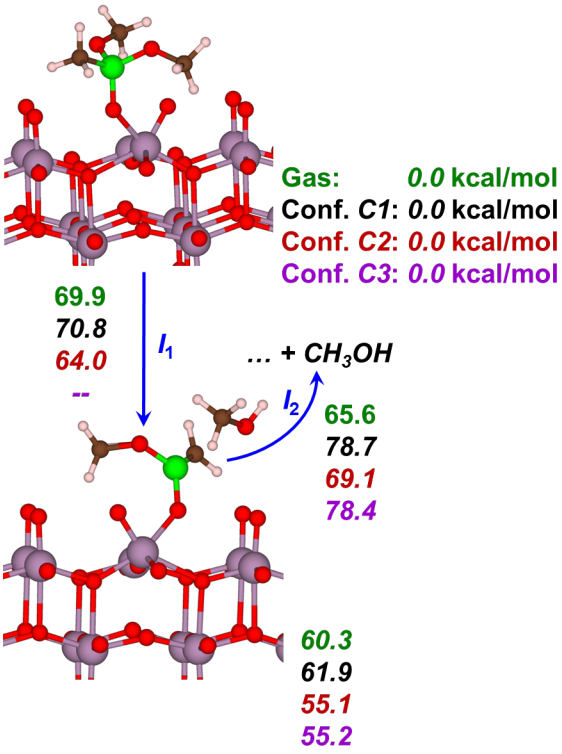

Figure 7. Schematic representation of the methanol formation via intramolecular hydrogen transfer on the pristine MoO_3 (010) surface (configurations *C1* and *C2*) and surface containing oxygen vacancies (configuration *C3*). Obtained energies are shown in kcal/mol.

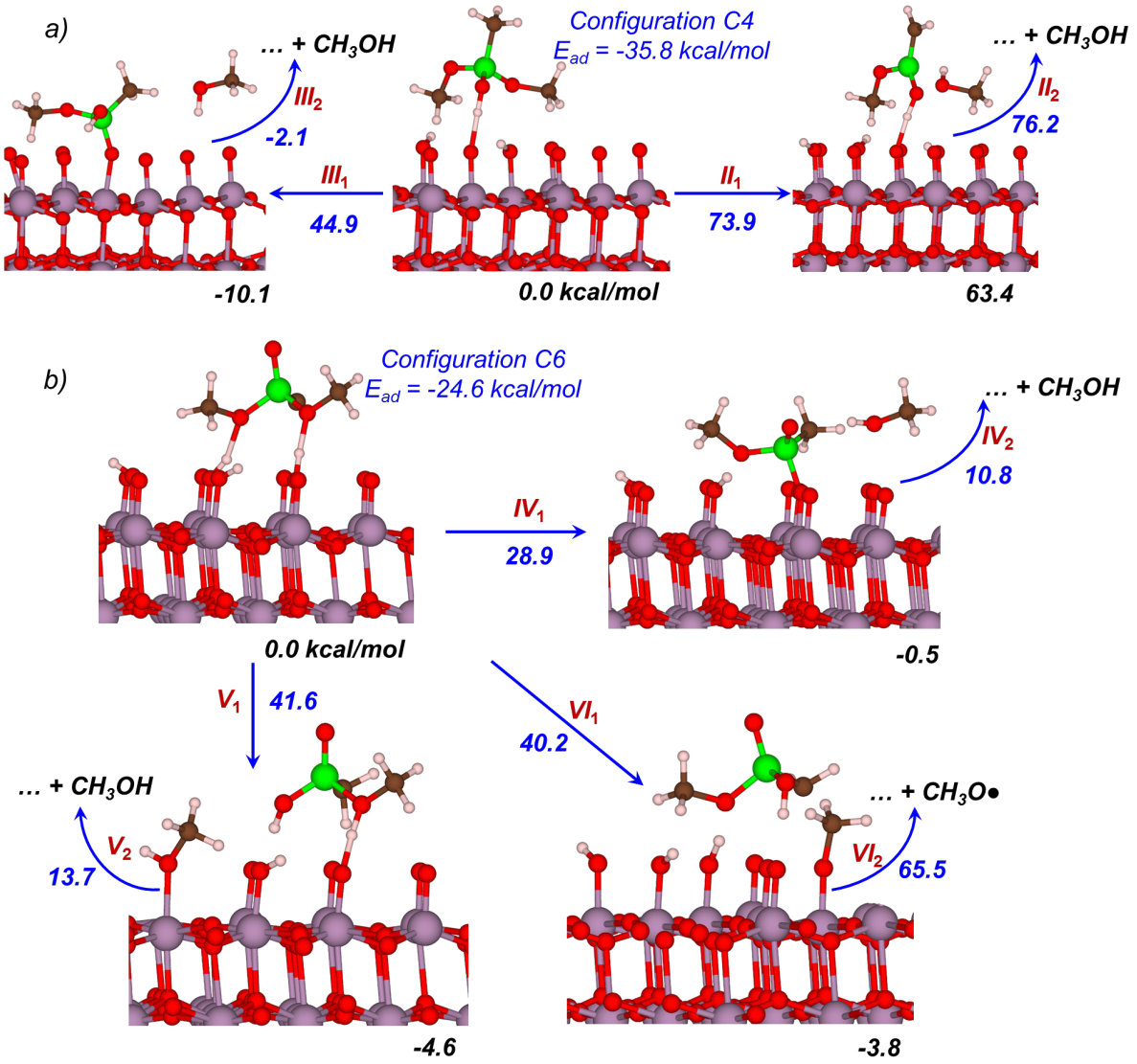

Figure 8. Possible mechanisms for the methanol elimination from DMMP adsorbed on the hydroxylated (010) MoO_3 surface starting from a) configuration *C3* and b) configuration *C5*. All obtained energies are shown in kcal/mol. The black numbers are in reference to the lowest energy structure labelled 0.0 kcal/mol. The blue numbers over arrows are activation energies.

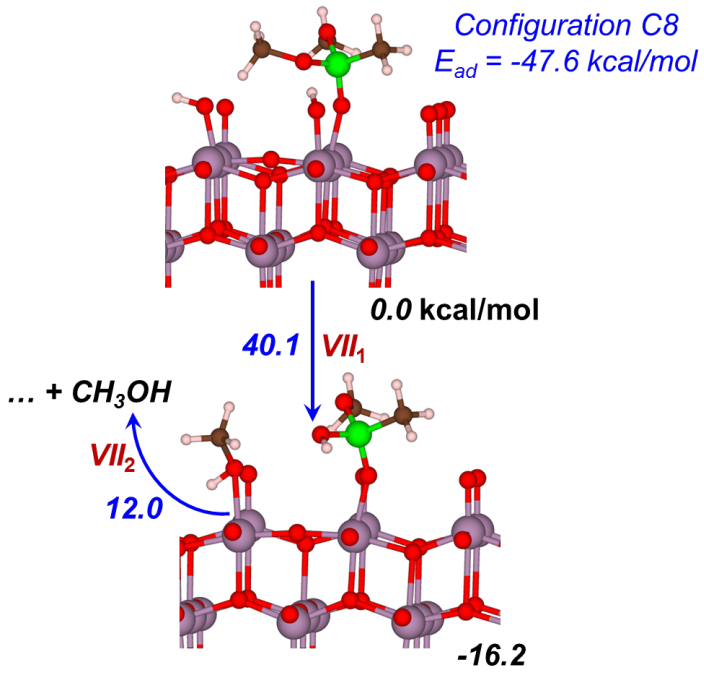

Figure 9. Mechanisms for the methanol elimination from DMMP adsorbed on the (010) MoO_3 surface containing oxygen vacancy and hydroxyl groups (configuration *C8*, Figure 8h). All obtained energies are shown in kcal/mol. The black numbers are in reference to the lowest energy structure labelled 0.0 kcal/mol. The blue numbers over arrows are activation energies.

Discussion

The low DMMP coverage on MoO_3 shown in Figure 5b suggests that adsorption is not strongly occurring, especially on pristine MoO_3 at lower pressures, which is also seen in the DFT calculations that show a weak interaction of the phosphoryl oxygen with the terminal surface O atoms (cf. Figure 6a). The most favored organophosphonate interaction with other metal oxides, such as TiO_2, Al_2O_3, Fe_2O_3, and Y_2O_3, is proposed to be between the phosphoryl group and under-coordinated Lewis acid metal sites.[4,6,7,9-11,12,16,18,84] The lack of Lewis acid metal sites inherent to the structure of the stoichiometric MoO_3(010) surface leads to weak adsorption of DMMP. Oxygen

vacancies (that generate Mo^{5+} sites) would provide the ideal binding sites for DMMP, and, indeed, the calculations here predict favorable energies for DMMP adsorption on oxygen vacancies. However, although calculations show that DMMP binds to both Mo^{5+} and hydroxyl groups (both present on OH-MoO_3) more strongly than to pristine MoO_3, it is difficult to assess the contribution of the Mo^{5+} to DMMP adsorption in these experiments. . While it is possible that DMMP is binding to Mo^{5+} sites, we suggest that hydroxyl groups are also playing a role in the increased adsorption of DMMP. Hydroxyl groups are expected to be the next favorable site for DMMP adsorption onto other metal oxides.[4-7,9-11,15,16] Typically, hydroxyl groups form at oxygen vacancies of metal oxides by the dissociation of water and oxidation of the metal;[73] it is likely that this process is occurring on some of the Mo^{5+} sites after sputtering. Our calculated adsorption energies in Figure 6 support hydroxyl groups as favorable adsorption sites. Figure 6e shows another possible adsorption structure on a hydroxylated surface that has not been considered previously, where hydrogen bonds between both methoxy oxygen atoms and two surface hydroxyl groups result in a configuration with an adsorption energy that is 0.5 eV higher than the lowest energy structure.

The binding energy difference between the functional groups in the C 1s and O 1s spectra as well as the presence of only a single P species in the P 2p spectrum demonstrate strong similarities between adsorbed and gas phase DMMP.[36] However, the C 1s spectra indicate methoxy group loss, especially for OH-MoO_3. DFT calculations (Table 1 and Figures 8 and 9) show the plausible adsorption configurations of DMMP on OH-MoO_3 have energetically favorable pathways to form methanol, while decomposition on oxygen vacancy sites was found to not be favorable unless there is a neighboring hydroxyl group. Evidence of the remaining molecular fragments is not seen in any of the spectra. While the binding energies of the possible dissociation products are not known, it is likely that they are similar to those of the intact DMMP molecule.[3] Our calculations show that methanol should easily desorb from the surface. TPD[24,26,85-87] and IR spectroscopy[85,87,88,89] studies indicate that methanol both adsorbs weakly intact and forms surface methoxy groups, but the presence of hydroxyl groups on the starting surface is not

addressed. However, while the adsorption is known to be affected by the crystalline phase and defects,[24] methanol does not readily adsorb onto stiochiometric MoO_3(010).[85] The binding energies of both adsorbed methanol and surface-bound methoxy groups are indistinguishable from adsorbed DMMP; therefore, these possibilities cannot be excluded. The C 1s methoxy:methyl peak area ratio is clearly less than the predicted 2:1 for the intact molecule, indicating at least some methanol is desorbing. The adsorbed water on the OH-MoO_3 surface could influence the amount of methanol that is formed. DMMP is known to hydrolyze in water to form methanol and methyl phosphonic acid.[1] This reaction combined with desorbing methanol product may be the reason the C 1s peak area ratio is the lowest at low DMMP pressure for OH-MoO_3. In addition to methanol loss, a cleavage of the O-CH_3 bond requires noticeably lower energy on the OH-MoO_3 surface (Table 1); however, our experimental results neither confirm nor exclude this possibility.

These results complement recent work by Tang and coworkers on DMMP adsorption on size-selected $(MoO_3)_3$ clusters.[90] They found that DMMP adsorbs onto the clusters in a similar configuration and calculated enhanced adsorption onto hydroxylated clusters. Similarly, they found that that stoichiometric clusters did not decompose DMMP but calculations suggest hydroxyl groups lower the energy required for decomposition by four-fold. The O-CH_3 bond dissociation energy was also found to be one of the lowest energy processes among Equations 1 through 4.

The amount of Mo^{5+} on the MoO_3 sample increases with DMMP pressure, as is shown in the Mo 3d spectra in Figure 2b. This increase is gradual with the pressure and not a result of damage by the photon beam. Simple alcohols have been shown to reduce MoO_3[91] and have been used in reduced MoO_3 sample preparations.[92] MoO_3 by itself, on other metal oxide supports, and mixed in a ferric molybdenate is used in methanol oxidation catalysis where Mo is the oxidant. Chung and coworkers found that Mo was not reduced until 110 ºC.[88] However if methanol is being formed and then further reacting to form surface methoxy groups, perhaps Mo reduction is occurring in this system. The Mo 3d spectrum of OH-MoO_3 does not change with DMMP pressure; the larger extent of Mo reduction before DMMP exposure is likely the reason.

Conclusions

APXPS studies were conducted in parallel with theoretical calculations to determine the room temperature adsorption behavior and decomposition of DMMP on a polycrystalline MoO_3 surface, including elucidation of the role of oxygen vacancies, hydroxyl groups and molecularly adsorbed water. APXPS data combined with DFT calculations have revealed that DMMP binds weakly to MoO_3. Introducing oxygen vacancies on the MoO_3 results in an increase in hydroxyl groups and adsorbed molecular water on the surface. DFT calculations and the surface coverages calculated from the APXPS data suggest that the oxygen vacancies and hydroxyl groups enhance the adsorption of DMMP, but it is difficult to separate the contributions of the two features in the APXPS data. With the C 1s spectra indicating a loss of methoxy carbon, it is highly likely that methanol is forming and desorbing from the surface, facilitated by the increase of hydroxyl groups and molecular water on the surface. Methanol may also adsorb on the MoO_3 surface, reducing the Mo^{6+}. These findings are consistent with previous proposals of under-coordinated metal atoms and hydroxyl groups being favored surface adsorption sites for DMMP on metal oxides. The results of this study build on results from a parallel study of DMMP adsorption on $(MoO_3)_3$ clusters,[90] showing how the adsorption behavior scales from the nanoregime to bulk oxide films.

Supporting Information. Additional spectra addressing photon-induced sample damage, spectral fits, DMMP coverage calculations, and additional theoretical calculations. This material is available free of charge via the Internet at http://pubs.acs.org.

Corresponding Author

* E-mail mkukla@nsf.gov, Tel 703-292-4940 (M.M.K.).

*E-mail hbluhm@lbl.gov, Tel 510-486-5431 (H.B.).

Notes

The authors declare no competing financial interest.

ACKNOWLEDGMENT

This work was funded by the Department of Defense (Grant HDTRA11510005). R.T. and M.M.K acknowledge support from NSF XSEDE resources (Grant DMR-130077) and DOE NERSC resources (Contract DE-AC02-05CH11231) and computational resources at the Maryland Advanced Research Computing Center (MARCC). MMK is grateful to the Office of the Director of National Science Foundation for support under the Independent Research and Development program. Any appearance of findings, conclusions, or recommendations expressed in this material are those of the authors and do not necessarily reflect the views of NSF. The Advanced Light Source is supported by the Director, Office of Science, Office of Basic Energy Sciences, of the U.S. Department of Energy under Contract No. DE-AC02-05CH11231.

ABBREVIATIONS

APXPS, ambient pressure X-ray photoelectron spectroscopy; DMMP, dimethyl methylphosphonate; L, Langmuir; PE, photoemission; XPS, X-ray photoelectron spectroscopy.

Table of Contents Graphic

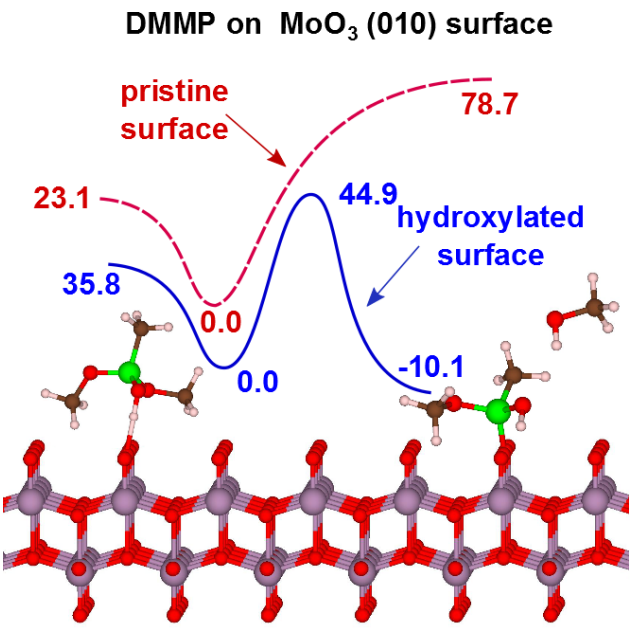

REFERENCES

[1] Kim, K.; Tsay, O. G.; Atwood, D. A.; Churchill, D. G. Destruction and Detection of Chemical Warfare Agents. *Chem. Rev.* **2011,** *111,* 5345-5403.

[2] Aurian-Blajeni, B.; Boucher, M. M. Interaction of Dimethyl Methylphosphonate with Metal Oxides. *Langmuir* **1989,** *5*, 170-174.

[3] Zhou, J.; Varazo, K.; Reddic, J. E.; Myrick, M. L.; Chen, D. A. Decomposition of Dimethyl Methylphosphonate on TiO_2(110): Principal Component Analysis Applied to X-ray Photoelectron Spectroscopy. *Anal. Chim. Acta* **2003***, 496,* 289-300.

[4] Rusu, C. N.; Yates Jr., J. T. Adsorption and Decomposition of Dimethyl Methylphosphonate on TiO_2. *J. Phys. Chem. B* **2000,** *104,* 12292-12298.

[5] Kim, C. S.; Lad, R. J.; Tripp, C. P. Interaction of Organophosphorous Compounds with TiO_2 and WO_3 Surfaces Probed by Vibrational Spectroscopy. *Sensors and Actuators B* **2001***, 76,* 442-448.

[6] Panayotov, D. A.; Morris, J. R. Uptake of a Chemical Warfare Agent Simulant (DMMP) on TiO_2: Reactive Adsorption and Active Site Poisoning. *Langmuir* **2009,** *25*, 3652-3658.

[7] Panayotov, D. A.; Morris, J. R. Thermal Decomposition of a Chemical Warfare Agent Simulant (DMMP) on TiO_2: Adsorbate Reactions with Lattice Oxygen as Studied by Infrared Spectroscopy. *J. Phys. Chem. C* **2009,** *113,* 15684-15691.

[8] Moss, J. A.; Szczepankiewicz, S. H.; Park, E.; Hoffman, M. R. Adsorption and Photodegradation of Dimethyl Methylphosphonate Vapor at TiO_2 Surfaces. *J. Phys. Chem. B* **2005***, 109*, 19779-19785.

[9] Mitchell, M. B.; Sheinker, V. N.; Mintz, E. A. Adsorption and Decomposition of Dimethyl Methylphosphonate on Metal Oxides. *J. Phys. Chem. B* **1997,** *101,* 11192-11203.

[10] Templeton, M. K.; Weinberg, W. H. Adsorption and Decomposition of Dimethyl Methylphosphonate on an Aluminum Oxide Surface. *J. Am. Chem. Soc.* **1985,** *107,* 97-108.

[11] Templeton, M. K.; Weinberg, W. H. Decomposition of Phosphonate Esters Adsorbed on Aluminum Oxide. *J. Am. Chem. Soc.* **1985,** *107,* 774-779.

[12] Henderson, M. A.; Jin, T.; White, J. M. A TPD/AES Study of the Interaction of Dimethyl Methylphosphonate with α-Fe_2O_3 and SiO_2. *J. Phys. Chem.* **1986**, *90*, 4607-4611.

[13] Tesfai, T. M.; Scheinker, V. N.; Mitchell, M. B. Decomposition of Dimethyl Methylphosphonate (DMMP) on Alumina-Supported Iron Oxide. *J. Phys. Chem. B* **1998**, *102*, 7299-7302.

[14] Chen, D. A.; Ratliff, J. S.; Hu, X.; Gordon, W. O.; Senanayake, S. D.; Mullins, D. R. Dimethyl Methylphosphonate Decomposition on Fully Oxidized and Partially Reduced Ceria Thin Films. *Surf. Sci.* **2010**, *604*, 574-587.

[15] Kanan, S. M.; Tripp, C. P. An Infrared Study of Adsorbed Organophosphonates on Silica: A Prefiltering Strategy of the Detection of Nerve Agents on Metal Oxide Sensors. *Langmuir* **2001**, *17,* 2213-2218.

[16] Gordon, W. O.; Tissue, B. M.; Morris, J. R. Adsorption and Decomposition of Dimethyl Methylphosphonate on Y_2O_3 Nanoparticles. *J. Phys. Chem. C* **2007,** *111,* 3233-3240.

[17] Cao, L.; Segal, S. R.; Suib, S. L.; Tang, X.; Satyapal, S. Thermocatalytic Oxidation of Dimthyl Methylphosphonate on Supported Metal Oxides. *J. Catal.* **2000**, *194*, 61-70.

[18] Mitchell, M. B.; Sheinker, V. N.; Cox Jr., W. W.; Gatimu, E. N.; Tesfamichael, A. B. The Room Temperature Decomposition Mechanism of Dimthyl Methylphosphonate (DMMP) on Alumina-Supported Cerium Oxide – Participation of Nano-Sized Cerium Oxide Domains. *J. Phys. Chem. B* **2004**, *108,* 1634-1645.

[19] Hermann, K.; Witko, M. Theory of physical and chemical behavior of transition metal oxides: vanadium and molybdenum oxides. In *Oxide Surfaces*, Woodruff, D. P., Ed., Elsevier Science B. V.: Amersterdam, 2001; Ch. 4, pp 136-198.

[20] Coquet, R.; Willock, D. J. The (010) Surface of α-MoO_3, a DFT + U Study. *Phys. Chem. Chem. Phys.* **2005,** *7,* 3819-3828.

[21] Yin, X.; Han, H.; Miyamoto, A. Structure and Adsorption Properties of MoO_3: Insights from Periodic Density Functional Calculations. *J. Mol. Model* **2001**, *7*, 207-215.

[22] Yan, Z.; Zuo, Z. Lv, X.; Li, Z.; Li, Z.; Huang, W. Adsorption of NO on MoO_3(010) Surface with Different Location of Terminal Oxygen Vacancy Defects: A Density Functional Theory Study. *Appl. Surf. Sci.* **2012,** *258,* 3136-3167.

[23] Hermann, K.; Witko, M.; Michalak, A. Density Functional Studies of the Electronic Structure and Adsorption at Molybdenum Oxide Surfaces. *Catal. Today* **1999,** *50,* 567-577.

[24] O'Brien, M. G.; Beale, A. M.; Jacques, S. D. M.; Buslaps, T.; Honkimaki, V.; Weckhuysen, B. M. On the Active Oxygen in Bulk MoO_3 During the Anaerobic Dehydrogenation of Methanol. *J. Phys. Chem. C* **2009,** *113,* 4890-4897.

[25] Rousseau, R.; Dixon, D. A.; Kay, B. D.; Dohnálek, Z. Dehydration, Dehydrogenation, and Condensation of Alcohols on Supported Oxide Catalysts Based on Cyclic $(WO_3)_3$ and $(MoO_3)_3$ Clusters. *Chem. Soc. Rev.* **2014,** *43,* 7664-7680.

[26] Bowker, M.; Carley, A. F.; House, M. Contrasting the Behaviour of MoO_3 and MoO_2 for the Oxidation of Methanol. *Catal. Lett.* **2008,** *120,* 34-39.

[27] Ressler, T.; Wienold, J.; Jentoft, R. E.; Girgsdies, F. Evolution of Defects in the Bulk Structure of MoO_3 During the Catalytic Oxidation of Propene. *Eur. J. Inorg. Chem.* **2003**, 301-312.

[28] Tokarz-Sobieraj, R.; Hermann, K.; Witko, M.; Blume, A.; Mestl, G.; Schlögl, R. Properties of Oxygen Sites at the MoO_3(010) Surface: Density Functional Theory Cluster Studies and Photoemission Experiments. *Surf. Sci.* **2001**, *489*, 107-125.

[29] Starr, D. E.; Liu, Z.; Hävecker, M.; Knop-Gericke, A.; Bluhm, H. Investigation of Solid/vapor Interfaces Using Ambient Pressure X-ray Photoelectron Spectroscopy. *Chem. Soc. Rev.* **2013**, *42*, 5833-5857.

[30] Head, A. R.; Bluhm, H. *Ambient Pressure X-Ray Photoelectron Spectroscopy* in "Reference Module in Chemistry, Molecular Sciences and Chemical Engineering", Jan Reedijk (Ed.), Elsevier B. V. (2016)

[31] Bluhm, H. Photoelectron Spectroscopy of Surfaces under Humid Conditions. *J. Electron Spectrosc. Rel. Phenom.* **2010**, 177, 71-84.

[32] Bluhm, H.; Hävecker, M.; Knop-Gericke, A.; Kiskinova, M.; Schlögl, R.; Salmeron, M. MRS Bull. **2007,** 32, 1022-1030.

[33] Bluhm, H.; Andersson, K.; Araki, T.; Benzerara, K.; Brown, G. E.; Dynes, J. J.; Ghosal, S.; Gilles, M. K.; Hansen, H.-Ch.; Hemminger, J. C.; et al. Soft X-ray Microscopy and Spectroscopy at the Molecular Environmental Science Beamline at the Advanced Light Source. *J. Electron Spectrosc. Related Phenom.* **2006**, *150,* 86-104.

[34] Ogletree, D. F.; Bluhm, H., Lebedev, G.; Fadley, C. S.; Hussain, Z.; Salmeron, M. A Differentially Pumped Electrostatic Lens System for Photoemission Studies in the Millibar Range. *Rev. Sci. Instrum.* **2002**, *73*, 3872-3877.

[35] Scanlon, D. O.; Watson, G. W.; Payne, D. J.; Atkinson, G. R.; Egdell, R. G.; Law, D. S. L. Theoretical and Experimental Study of the Electronic Structure of MoO_3 and MoO_2. *J. Phys. Chem. C* **2010,** *114*, 4636-4645.

[36] Head, A. R.; Tsyshevsky, R.; Trotochaud, L.; Eichhorn, B.; Kuklja, M. M.; Bluhm, H. Electron Spectroscopy and Computational Studies of Dimethyl Methylphosphonate. *J. Phys. Chem. A* **2016**, *120,* 1985-1991.

[37] Smith, R. L.; Rohrer, G. S. An Atomic Force Microscopy Study of the Morphological Evolution of the MoO3 (010) Surface during Reduction Reactions. *J. Catal.* **1996**, *163*, 12–17.

[38] Firment, L. E.; Ferretti, A. Stoichiometric and Oxygen Deficient MoO_3(010) Surfaces. *Surf. Sci.* **1983**, *129*, 155-176.

[39] Hermann, K.; Michalak, A.; Witko, M. Cluster Model Studies on Oxygen Sites at the (010) Surfaces of V_2O_5 and MoO_3. *Catal. Today* **1996**, *32*, 321-327.

[40] Lei, H.; Chen, Z.-X. Density Functional Studies of the Electronic Structure and Adsorption at Molybdenum Oxide Sites. *J. Phys. Chem. C* **2012**, *116*, 25757 –25764.

[41] Chen, M.; Waghmare, U. V.; Friend, C. M.; Kaxiras, E. A Density Functional Study of Clean and Hydrogen-Covered α-MoO_3 (010): Electronic structure and surface relaxation. *J. Chem. Phys.* **1998**, *109*, 6854-6860.

[42] Negishi, H.; Negishi, S.; Kuroiwa, Y.; Sato, N.; Aoyagi, S. Anisotropic Thermal Expansion of Layered MoO_3 Crystals. *Phys. Rev. B.* **2004**, *69*, 064111.

[43] Sitepu, H. Texture and Structural Refinement Using Neutron Diffraction Data from Molybdite (MoO_3) and Calcite ($CaCO_3$) Powders and a Ni-rich $Ni_{50.7}Ti_{49.30}$ Alloy. *Powder Diffr.* **2009**, *24*, 315–326.

[44] Hohenberg, P.; Kohn, W. Inhomogeneous Electron Gas, *Phys. Rev.* **1964**, *136,* B864-B871.

[45] Kohn, W.; Sham, L. J. Self-Consistent Equations Including Exchange and Correlation Effects, *Phys. Rev.* **1965**, *140,* A1133-A1138.

[46] Ding, H.; Ray, K. G.; Ozolins, V.; Asta, M. Structural and vibrational properties of α-MoO3 from van derWaals corrected density functional theory calculations, *Phys. Rev.B* **2012**, *85,* 012104.

[47] Inzani, K.; Grande, T.; Vullum-Bruer, F.; Selbach, S. M. A van der Waals Density Functional Study of MoO3 and Its Oxygen Vacancies, *J. Phys. Chem. C* **2016**, *120*, 8959−8968.

[48] Dion, M.; Rydberg, H.; Schröder, E.; Langreth, D. C.; Lundqvist, B. I. Van der Waals Density Functional for General Geometries, *Phys. Rev. Lett.* **2004**, *92,* 246401.

[49] Thonhauser, T.; Cooper, V. R.; Li, S.; Puzder, A.; Hyldgaard, P.; Langreth, D. C. Van der Waals Density Functional: Self-Consistent Potential and the Nature of the van der Waals Bond. *Phys. Rev. B* **2007,** *76*, 125112.

[50] Román-Pérez, G.; Soler, J. M. Efficient Implementation of a van der Waals Density Functional: Application to Double-Wall Carbon Nanotubes. *Phys. Rev. Lett.* **2009,** *103*, 096102.

[51] Klimeš, J.; Bowler, D. R.; Michaelides, A. Chemical Accuracy for the Van der Waals Density Functional. *J. Phys.: Cond. Matt.* **2009**, *22*, 022201-1-5.

[52] KlimešRomán-Pérez, G.; Soler, J.; Bowler, D. R.; Michaelides, A. Van. M. Efficient Implementation of a van der Waals Density Functionals AppliedFunctional: Application to Solids.Double-Wall Carbon Nanotubes. *Phys. Rev. B* **2011**, *83*, 195131*Lett.* **2009,** *103*, 096102.

[53] Kresse, G.; Futhmüller, J. Efficiency of ab-initio Energy Calculations for Metals and Semiconductors Using a Plane-Wave Basis Set. *Comput. Mater. Sci.* **1996**, *6*, 15-50.

[54] Kresse, G.; Furthmüller, F. Efficient Iterative Schemes for ab initio Total-Energy Calculations Using a Plane-Wave Basis Set. *Phys. Rev. B* **1996,** *54*, 11169-11186.

[55] Kresse, G.; Hafner, J. Ab initio Molecular Dynamics for Liquid Metals. *Phys. Rev. B* **1993**, *47,* 558-561.

[56] Blöchl, P. E. Projector Augmented-Wave Method. *Phys. Rev. B* **1994,** *50,* 17953-17979.

[57] Negishi, H.; Negishi, S.; Kuroiwa, Y.; Sato, N.; Aoyagi, S. Anisotropic Thermal Expansion of Layered MoO_3 Crystals. *Phys. Rev. B*. **2004**, *69*, 064111.

[58] Sitepu, H. Texture and Structural Refinement Using Neutron Diffraction Data from Molybdite (MoO_3) and Calcite ($CaCO_3$) Powders and a Ni-rich $Ni_{50.7}Ti_{49.30}$ Alloy. *Powder Diffr*. **2009**, *24*, 315–326.

[59] Lei, Y.-H.; Chen, Z.-X. A Theoretical Study of Stability and Vacancy Replenishing of MoO_3(010) Surfaces in Oxygen Atmosphere. *Appl. Surf. Sci*. **2016**, *361*, 107-103.

[60] Perdew, J. P.; Burke, K.; Ernzerhof, M. Generalized Gradient Approximation Made Simple. *Phys. Rev. Lett*. **1996**, *77*, 3865-3868.

[61] Dudarev, S. L.; Savrasov, S. Y.; Humphreys, C. J.; Sutton, A. P. Electron-Energy-Loss Spectra and the Structural Stability of Nickel Oxide: An LSDA+U Study, *Phys. Rev. B* **1998**, *57*, 1505–1509.

[62] Becke, A. D. Density-Functional Thermochemistry. 3. The Role of Exact Exchange. *J. Chem. Phys*. **1993**, *98*, 5648-5652.

[63] Lee, C.; Yang, W.; Parr, R. G. Development of the Colle-Salvetti Correlation-Energy Formula into a Functional of the Electron- Density *Phys. Rev. B*, **1988,** *37*, 785-789.

[64] M.J. Frisch, G.W. Trucks, H.B. Schlegel, G.E. Scuseria, M.A. Robb, J.R. Cheeseman, G. Scalmani, V. Barone, B. Mennucci, G.A. Petersson, et al Gaussian 09, in, Gaussian, Inc., Wallingford, CT, USA, 2009.

[65] Henkelman, G.; Uberuaga, B. P.; Jónsson, H. A Climbing Image Nudged Elastic Band Method for Finding Saddle Points and Minimum Energy Paths. *J. Chem. Phys.* **2000**, *113*, 9901-9904.

[66] Hratchian, H. P.; Schlegel, H. B. Accurate reaction paths using a Hessian based predictor-corrector integrator. *J. Chem. Phys.* **2004**, *120*, 9918-9924.

[67] Hratchian, H. P.; Schlegel, H. B. Using Hessian Updating to Increase the Efficiency of a Hessian based predictor-corrector reaction path following method", Based Predictor-Corrector Reaction Path Following Method. *J. Chem. Theory Comput.* **2005**, *1,* 61-69.

[68] Ramana, C. V.; Atuchin, V. V.; Kesler, V. G.; Kochubey, V. A.; Pokrovsky, L. D.; Shutthanandan V.; Becker, U.; Ewing, R. C. Growth and Surface Characterization of Sputter-Deposited Molybdenum Oxide Thin Films. *Appl. Surf. Sci.* **2007**, *253*, 5368-5374.

[69] Song, Z.; Cai, T.; Chang, Z.; Liu, G.; Rodriguez, J. A.; Hrbek, J. Molecular Level Study of the Formation and the Spread of MoO_3 on Au(111) by Scanning Tunneling Microscopy and X-ray Photoelectron Spectroscopy. *J. Am. Chem. Soc.* **2003,** *125,* 8059-8066.

[70] Choi, J.-G.; Thompson, L. T. XPS Study of As-prepared and Reduced Molybdenum Oxides. *Appl. Surf. Sci.* **1996,** *93*, 143-149.

[71] Brox, B.; Olefjord, I. ESCA Studies of MoO_2 and MoO_3. *Surf. Inter. Anal.* **1988,** *13*, 3-6.

[72] Liao, X.; Jeong, A. R.; Wilks, R. G.; Wiesner, S.; Rusu, M.; Bär, M. X-ray Irradiation Induced Effects on the Chemical and Electronic Peoperties of MoO_3 Thin Films. *J. Electron Spectrosc. Rel. Phenom.,* 2016, **212**, 50-55.

[73] Ketteler, G.; Yamamoto, S.; Bluhm, H.; Andersson, K.; Starr, D. E.; Ogletree, D. F.; Ogasawara, H.; Nilsson, A.; Salmeron, M. The Nature of Water Nucleation Sites on TiO_2(110) Surfaces Revealed by Ambient Pressure X-ray Photoelectron Spectroscopy. *J. Phys. Chem. C* **2007,** *111,* 8278-8282.

[74] Newberg, J. T.; Starr, D. E.; Yamamoto, S.; Kaya, S.; Kendelewicz, T.; Mysak, E. R.; Porsgaard, S.; Salmeron, M. B.; Brown Jr., G. E.; Nilsson, A. et al. Formation of Hydroxyl and Water Layers on MgO Films Studied with Ambient Pressure XPS. *Surf. Sci.* **2011**, *605*, 89-94.

[75] Zeng, H. C.; Xie, F.; Wong, K. C.; Mitchell, K. A. R. Insertion and Removal of Protons in Single-Crystal Orthorhomic Molybdenum Trioxide under H_2S/H_2 and O_2/N_2. *Chem. Mater.* **2002**, *14*, 1788-1796.

[76] Sian, T. S.; Reddy, G. B. Effect of Stoichiometry and microstructure on Hydrolysis in MoO_3 Films. Chem. Phys. Lett. **2006**, 418, 170-173.

[77] Dufour, L. C.; Bertrand, O.; Floquet, N. Chemical Reactivity of (010)MoO_3: A Structural Study of the MoO_2 Formation in Molecular Hydrogen. *Surf. Sci.* **1984,** 147, 396-412.

[78] Ketteler, G.; Yamamoto, S.; Bluhm, H.; Andersson, K.; Starr, D. E.; Ogletree, D. F.; Ogasawara, H.; Nilsson, A.; Salmeron, M. The Nature of Water Nucleation Sites on TiO_2(110) Surfaces Revealed by Ambient Pressure X-ray Photoelectron Spectroscopy. *J. Phys. Chem. C* **2007,** *111,* 8278-8282.

[79] Newberg, J. T.; Starr, D. E.; Yamamoto, S.; Kaya, S.; Kendelewicz, T.; Mysak, E. R.; Porsgaard, S.; Salmeron, M. B.; Brown Jr., G. E.; Nilsson, A. et al. Formation of Hydroxyl and Water Layers on MgO Films Studied with Ambient Pressure XPS. *Surf. Sci.* **2011**, *605*, 89-94.

[80] Henderson, M. A. *Surf. Sci. Rep.* **2002,** *46*, 1-308.

[81] Kim, Y. J.; Gao, Y.; Chambers, S. A. Core-level X-ray Photoelectron Spectra and X-ray Photoelectron Diffraction of RuO_2(110) Grown by Molecular Beam Epitaxy. *Appl. Surf. Sci.* **1997**, *120*, 250-260.

[82] Yamamoto, S.; Andersson, K.; Bluhm, H.; Ketteler, G.; Starr, D. E.; Schiros, T.; Ogasawara, H.; Pettersson, L. G. M.; Salmeron, M.; Nilsson A. *J. Phys. Chem. C* **2007**, *111*, 7848-7850.

[83] Liang, S.; Hemberger, P.; Neisius, N. M.; Bodi, A.; Grützmacher, H.; Levalois- Grützmacher, J.; Gaan, S. Elucidating the Thermal Decomposition of Dimethyl Methylphosphonate by Vacuum Ultraviolet (VUV) Photoionization: Pathways to the PO Radical, a Key Species in Flame-Retardant Mechanisms. *Chem. Eur. J.* **2015**, *21*, 1073 – 1080.

[84] Kuiper, A. E. T.; van Bokhoven, J. J. G. M.; Medema, J. The Role of Heterogeneity in the Kinetics of a Surface Reaction I. Infrared Characterization of the Adsorption Structures of Organophosphonates and Their Decomposition. *J. Catal.* **1976,** *43,* 154-167.

[85] Chowdhry, U.; Ferretti, A.; Firment, L. E.; Machiels, C. J.; Ohuchi, F.; Sleight, A. W.; Staley, R. H. Mechanism and Surface Structural Effects in Methanol Oxidation over Molybdates. *Appl. Surf. Sci.* **1984***, 19*, 360-372.

[86] Farneth, W. E.; Ohuchi, F.; Staley, R. H.; Chowdhry, U.; Sleight, A. W. Mechanism of Partial Oxidation of Methanol over MoO_3 as Studied by Temperature-Programmed Desorption. *J. Phys. Chem.* **1985**, *89*, 2493-2497.

[87] Street, S. C.; Goodman, D. W. Chemical and Spectroscopic Surface Science Investigation of MoO_3 and MoO_3/Al_2O_3 Ultrathin Films. *J. Vac. Sci. Technol. A* **1997**, *15*, 1717-1723.

[88] Chung, J. S.; Miranda, R.; Bennett, C. O. Study of Methanol and Water Chemisorbed on Molybdenum Oxide. *J. Chem. Soc., Faraday Trans. 1* **1985***, 81*, 19-36.

[89] Groff, R. P. An Infrared Study of Methanol and Ammonia Adsorption on Molybdenum Trioxide. *J. Catal.* **1984**, *86,* 215-218.

[90] Tang, X.; Hicks, Z.; Wang, L.; Ganteför, G.; Fairbrother, D. H.; Bowen, K. H.; Tsyshevsky, R.; Sun, J.; Kuklja, M. M. Decomposition of Dimethyl Methylphosphonate by Size-Selected $(MoO_3)_3$ Clusters *submitted*

[91] Farneth, W. E.; Staley, R. H.; Sleight, A. W. Stoichiometry and Structural Effects in Alcohol Chemisorption /Temperature-Programmed Desorption on MoO_3. *J. Am. Chem. Soc.* **1986**, *108*, 2327-2332.

[92] Li, T.; Beidaghi, M.; Xiao, X.; Huang, L.; Hu, Z.; Sun, W.; Chen, X.; Gogotsi, Y.; Zhou, J. Ethanol Reduced Molybdenum Trioxide for Li-ion Capacitors. *Nano Energy* **2016,** *26* 100-107.